A Letters Journal Exploring the Frontiers of Physics

January 2023

EPL, **141** (2023) 16001
doi: 10.1209/0295-5075/acabe1

www.epljournal.org

Effective medium theory with hybrid impacts of phase symmetry and asymmetry for analyzing phase transition behavior

X. C. Zhou[1,2,3], W. Y. Lin[2,4], F. B. Yang[1,2,3], X. D. Zhou[2,4,5,6], J. Shen[1,2,4,5,6,7,8] and J. P. Huang[1,2,3(a)]

[1] *Department of Physics, Fudan University - Shanghai 200438, China*
[2] *State Key Laboratory of Surface Physics, Fudan University - Shanghai 200438, China*
[3] *Key Laboratory of Micro and Nano Photonic Structures (MOE), Fudan University - Shanghai 200438, China*
[4] *Institute for Nanoelectronic Devices and Quantum Computing, Fudan University - Shanghai 200438, China*
[5] *Shanghai Qi Zhi Institute - Shanghai 200232, China*
[6] *Zhangjiang Fudan International Innovation Center, Fudan University - Shanghai 201203, China*
[7] *Shanghai Research Center for Quantum Sciences - Shanghai 200433, China*
[8] *Collaborative Innovation Center of Advanced Microstructures - Nanjing 210093, China*

received 9 September 2022; accepted in final form 15 December 2022
published online 4 January 2023

Abstract – Recent research found a hysteresis phenomenon of electric conductance against metallic phase ratio during the thermally driven metal-insulator transition in the vanadium trioxide system. Profoundly exploring the hysteresis mechanism might help analyze the phase transition behavior. However, there is no complete analytical theory to give a quantitative description. In this work, we developed an effective medium theory to predict the relationships between the effective electric conductance and the metallic phase ratio during warming and cooling processes. It reveals that the above hysteresis is due to the hybrid impacts of phase symmetry and asymmetry in spatial distribution (termed space factor). Then, we applied this theory to deduce the nucleation and growth behavior of the minority phase in the majority phase during phase transition. The predicted relationship between metallic phase ratio and temperature is consistent with the experimental results obtained by scanning microwave impedance microscopy. It shows that the above dynamic behaviors during the warming and cooling processes are asymmetrical (termed dynamic factor). Combining the space and dynamic factors, we summarized the thermal hysteresis mechanism of the metal-insulator transition. Finally, we analyzed the influence of these two factors on the electric conductance difference during the warming and cooling processes. The result indicates that adjusting asymmetrical elements in space and dynamic factors is key to controlling thermal hysteresis magnitude. Since the electric conductance in our theory can be replaced by other physical properties, such as thermal conductivity, dielectric constant, and magnetic permeability, this work might help analyze many different phase transition behaviors.

Introduction. – Phase transitions, during which the macroscopic physical properties of the system might change significantly, are common in nature. People have used this phenomenon to achieve various applications, such as smart windows [1,2], energy storage [3–5], thermal diodes [6,7], and memory devices [8,9]. However, the phase transition processes in opposite directions are not entirely consistent [10,11]. Regarding the thermally driven phase transition, the macroscopic physical properties *vs.* temperature might differ during warming and cooling processes [12,13]. This phenomenon is called thermal hysteresis. Since there are specific requirements for the hysteresis magnitude in practical applications, such as shape memory and thermal utilization, studying the hysteresis mechanism can help to analyze the phase transition behavior and promote technology development [12,14–16].

Vanadium trioxide (V_2O_3) is well known in various metal-insulator transition materials, with its electrical resistivity changing up to 10^6 magnitudes before and after the phase transition [17,18]. Recently, a strong thermal hysteresis has been directly visualized in the V_2O_3 system by scanning microwave impedance microscopy [19]. During the metal-insulator transition, the electric resistance R of the V_2O_3 sample in the warming process was

(a)E-mail: jphuang@fudan.edu.cn (corresponding author)

higher than that in the cooling process at the same temperature T. Researchers plotted the relationship between the metallic phase ratio $f_{\rm met}$ and T by analyzing the area fractions of the metallic and insulating phases. At the same T, $f_{\rm met}$ in the warming process was lower than in the cooling process. Yet, the thermal hysteresis is not entirely caused by the different $f_{\rm met}$. To go further, they plotted the relationship between the electric conductance G of the V_2O_3 sample and $f_{\rm met}$. The G in the warming process is almost the same as in the cooling process when $f_{\rm met} \to 50\%$, while the former is significantly lower than the latter when $f_{\rm met}$ is far from 50%. By analyzing the number of domains during the warming and cooling phase transitions, the researchers attributed the hysteresis of G against $f_{\rm met}$ to different domain evolutions [19]. That is, the domain distribution in the cooling process is easier for the current to pass through than in the warming process. In other words, the distribution of the metallic and insulating phases affects the macroscopic thermal hysteresis behavior. However, there is no complete quantitative analytical theory to explain this phenomenon. If we can describe the above process smoothly and comprehensively, we might understand thermal hysteresis more deeply.

As a powerful tool, effective medium theory (approximation) is widely used in thermal [20–22], optical [23–25], electrical [26,27], magnetic [28,29], and other systems [30, 31] to predict the macroscopic physical properties of composite materials according to the corresponding physical properties of each component. Considering the experimental explanation for the hysteresis of $G\,(f_{\rm met})$, we equate the domain evolution to the metallic and insulating phases in symmetrical and asymmetrical distributions. Fortunately, among various models of effective medium theory, there exist two basic formulas with symmetrical and asymmetrical characteristics. We smoothly combine them to predict the relationship between effective electric conductance $G_{\rm e}$ and $f_{\rm met}$ during the phase transition process. Comparing the theoretical predictions $G_{\rm e}\,(f_{\rm met})$ with the experimental results $G\,(f_{\rm met})$, we examine the accuracy of this method and reveal the hysteresis mechanism. We then apply the method to deduce the nucleation and growth behavior in the phase transition process. The predicting $f_{\rm met}(T)$ is validated by the experimental results obtained by scanning microwave impedance microscopy. Combining $G_{\rm e}\,(f_{\rm met})$ and $f_{\rm met}(T)$, we further analyze the thermal hysteresis mechanism of $G_{\rm e}(T)$. It guides controlling thermal hysteresis magnitude for practical applications.

Theory. – Maxwell-Garnett (M-G) formula [20,25,32–36] and Bruggeman formula [20,25,35–37] are fundamental in the effective medium theory, with asymmetrical and symmetrical characteristics, respectively. We apply them to calculate $G_{\rm e}$ in this study. Note that the V_2O_3 system in ref. [19] can be treated as a two-dimensional system, so we use the two-dimensional M-G and Bruggeman formulas. The M-G formula is suitable for solving the situation where inclusions are embedded in a host [32,33,38], as shown in fig. 1(a). For a two-dimensional isotropic binary composite, the M-G formula is

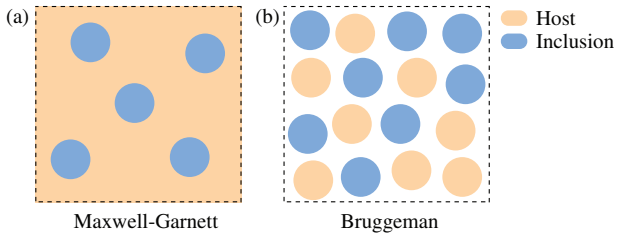

Fig. 1: Schematic diagram of (a) Maxwell-Garnett (M-G) formula for phase asymmetry and (b) Bruggeman formula for phase symmetry [25,38]. We use "host" and "inclusion" in the Bruggeman formula to make it consistent with the M-G formula in this work.

$$\frac{G_{\rm e,M\text{-}G} - G_{\rm h}}{G_{\rm e,M\text{-}G} + G_{\rm h}} = f_{\rm i}\frac{G_{\rm i} - G_{\rm h}}{G_{\rm i} + G_{\rm h}}, \tag{1}$$

where $G_{\rm e,M\text{-}G}$ is the effective electric conductance calculated by the M-G formula; $G_{\rm i}$ is the electric conductance of the inclusions; $G_{\rm h}$ is the electric conductance of the host; $f_{\rm i}$ is the area ratio of the inclusions [25,38]. This formula is asymmetrical. If we exchange the subscripts "i" and "h", $G_{\rm e,M\text{-}G}$ will differ. Thus, if the host and inclusions are non-exchangeable in the warming and cooling processes, we can use eq. (1) to calculate $G_{\rm e,M\text{-}G}$. For ease of presentation, we term the M-G formulas in the warming and cooling processes as M-G-1 and M-G-2 formulas, respectively. The Bruggeman formula is suitable for solving the situation where the inclusions and host are exchangeable [37,38], as shown in fig. 1(b). For a two-dimensional isotropic binary composite, the Bruggeman formula is

$$f_{\rm i}\frac{G_{\rm i} - G_{\rm e,B}}{G_{\rm i} + G_{\rm e,B}} + f_{\rm h}\frac{G_{\rm h} - G_{\rm e,B}}{G_{\rm h} + G_{\rm e,B}} = 0, \tag{2}$$

where $G_{\rm e,B}$ is the effective electric conductance calculated by the Bruggeman formula; $f_{\rm h}$ is the area ratio of the host; $f_{\rm i} + f_{\rm h} = 100\%$ [25,38]. This formula is symmetrical. If we exchange the subscripts "i" and "h", $G_{\rm e,B}$ will be the same. Since the applicable scopes of the M-G and Bruggeman formulas are different, it is necessary to develop a formula according to the characteristics of the metal-insulator transition in the warming and cooling processes.

For the warming process, we treat the phase transition process as a growth process of the metallic phase in the insulating phase. The metallic and insulating phases are considered the inclusions and host, respectively. Thus, we get the M-G formula in the warming process (M-G-1 formula),

$$\frac{G_{\rm e,M\text{-}G\text{-}1} - G_{\rm ins}}{G_{\rm e,M\text{-}G\text{-}1} + G_{\rm ins}} = f_{\rm met}\frac{G_{\rm met} - G_{\rm ins}}{G_{\rm met} + G_{\rm ins}}, \tag{3}$$

where $G_{\rm e,M\text{-}G\text{-}1}$ is the effective electric conductance calculated by the M-G-1 formula; $G_{\rm ins}$ is the electric

Table 1: Variations of η with $f_{\rm met}$ in the warming process.

$f_{\rm met}$	Formula	$G_{\rm e}$	η
0%	M-G-1	$G_{\rm e,M\text{-}G\text{-}1}$	1
$0\% \to 50\%$	M-G-1 + Bruggeman	$\eta G_{\rm e,M\text{-}G\text{-}1} + (1-\eta)G_{\rm e,B}$	$1 \to 0$
50%	Bruggeman	$G_{\rm e,B}$	0
$50\% \to 100\%$	M-G-1 + Bruggeman	$\eta G_{\rm e,M\text{-}G\text{-}1} + (1-\eta)G_{\rm e,B}$	$0 \to 1$
100%	M-G-1	$G_{\rm e,M\text{-}G\text{-}1}$	1

conductance of the insulating phase; $G_{\rm met}$ is the electric conductance of the metallic phase. The experimental data in ref. [19] shows that the electric conductances of the metallic and insulating phases depend on T: $G_{\rm met}(T)$ and $G_{\rm ins}(T)$. Meanwhile, $f_{\rm met}$ is related to T. There exist relationships between $G_{\rm met}$ and $f_{\rm met}$ ($G_{\rm ins}$ and $f_{\rm met}$): $G_{\rm met}\left(f_{\rm met}\right)$ and $G_{\rm ins}\left(f_{\rm met}\right)$. Then, the M-G-1 formula (eq. (3)) reads

$$\frac{G_{\rm e,M\text{-}G\text{-}1}\left(f_{\rm met}\right) - G_{\rm ins}\left(f_{\rm met}\right)}{G_{\rm e,M\text{-}G\text{-}1}\left(f_{\rm met}\right) + G_{\rm ins}\left(f_{\rm met}\right)} = f_{\rm met}\frac{G_{\rm met}\left(f_{\rm met}\right) - G_{\rm ins}\left(f_{\rm met}\right)}{G_{\rm met}\left(f_{\rm met}\right) + G_{\rm ins}\left(f_{\rm met}\right)}. \tag{4}$$

Moreover, we consider a situation where the inclusions and host are exchangeable, for instance, $f_{\rm i} = f_{\rm h} = 50\%$. We use the Bruggeman formula to treat this situation, which reads

$$f_{\rm met}\frac{G_{\rm met} - G_{\rm e,B}}{G_{\rm met} + G_{\rm e,B}} + f_{\rm ins}\frac{G_{\rm ins} - G_{\rm e,B}}{G_{\rm ins} + G_{\rm e,B}} = 0, \tag{5}$$

where $f_{\rm ins}$ is the insulating phase ratio. Considering $G_{\rm met}(f_{\rm met})$, $G_{\rm ins}(f_{\rm met})$, and $f_{\rm ins} + f_{\rm met} = 100\%$, the Bruggeman formula (eq. (5)) can be expressed as

$$f_{\rm met}\frac{G_{\rm met}\left(f_{\rm met}\right) - G_{\rm e,B}\left(f_{\rm met}\right)}{G_{\rm met}\left(f_{\rm met}\right) + G_{\rm e,B}\left(f_{\rm met}\right)} + \left(100\% - f_{\rm met}\right)\frac{G_{\rm ins}\left(f_{\rm met}\right) - G_{\rm e,B}\left(f_{\rm met}\right)}{G_{\rm ins}\left(f_{\rm met}\right) + G_{\rm e,B}\left(f_{\rm met}\right)} = 0. \tag{6}$$

Following the above analyses, we generally consider the sample has phase symmetry and phase asymmetry. The phase asymmetry is due to the non-exchangeability of the host and inclusions, which the M-G-1 formula can treat. Meanwhile, the phase symmetry is because of the exchangeability of the host and inclusions, which the Bruggeman formula can solve. Thus, the phase transition is a competitive process of phase symmetry and asymmetry. When the area ratios of the metallic phase and insulating phase are equal ($f_{\rm met} = f_{\rm ins} = 50\%$), the sample has complete phase symmetry. When the area ratio difference between the metallic phase and insulating phase reaches the maximum ($f_{\rm met} = 0\%, f_{\rm ins} = 100\%$ or $f_{\rm met} = 100\%, f_{\rm ins} = 0\%$), the sample has complete phase asymmetry. Then, we get three typical steps in the phase transition process: beginning, intermediate, and ending. The three typical steps can be expressed as

$$\begin{cases} f_{\rm met} = 0\%, \text{ beginning (complete phase asymmetry, M-G-1 formula);} \\ f_{\rm met} = 50\%, \text{ intermediate (complete phase symmetry, Bruggeman formula);} \\ f_{\rm met} = 100\%, \text{ ending (complete phase asymmetry, M-G-1 formula),} \end{cases} \tag{7}$$

where $f_{\rm met}$ satisfies $f_{\rm met} + f_{\rm ins} = 100\%$. Furthermore, the competition process of phase symmetry and asymmetry is continuous. When $f_{\rm met}$ increases from 0% to 50%, the complete phase asymmetry continuously changes to the complete phase symmetry. When $f_{\rm met}$ rises from 50% to 100%, the complete phase symmetry continuously changes to the complete phase asymmetry. It means that $G_{\rm e}\left(f_{\rm met}\right)$ should be decided by both $G_{\rm e,M\text{-}G\text{-}1}\left(f_{\rm met}\right)$ and $G_{\rm e,B}\left(f_{\rm met}\right)$. We define a weight parameter η for evaluating the contribution of $G_{\rm e,M\text{-}G\text{-}1}\left(f_{\rm met}\right)$ and $G_{\rm e,B}\left(f_{\rm met}\right)$ to $G_{\rm e}\left(f_{\rm met}\right)$. Thus, $G_{\rm e}\left(f_{\rm met}\right)$ can be expressed as

$$G_{\rm e}\left(f_{\rm met}\right) = \eta G_{\rm e,M\text{-}G\text{-}1}\left(f_{\rm met}\right) + (1-\eta)G_{\rm e,B}\left(f_{\rm met}\right). \tag{8}$$

More details about the variation of η with $f_{\rm met}$ are listed in table 1. When $f_{\rm met} \in [0\%, 50\%]$, the increasing $f_{\rm met}$ leads to the decreasing η. When $f_{\rm met} \in [50\%, 100\%]$, the increasing $f_{\rm met}$ causes the rising η. Following these rules and considering the three typical steps (eq. (7)), we assume that η satisfies

$$\eta = 4\left(f_{\rm met} - 50\%\right)^2. \tag{9}$$

For the cooling process, we regard the phase transition process as a growth process of the insulating phase in the metallic phase, which indicates that the insulating and metallic phases can be considered as the inclusions and host, respectively. Further analyzing $G_{\rm met}\left(f_{\rm met}\right)$, $G_{\rm ins}\left(f_{\rm met}\right)$, and $f_{\rm ins} + f_{\rm met} = 100\%$, we get the M-G formula in the cooling process (M-G-2 formula),

$$\frac{G_{\rm e,M\text{-}G\text{-}2}\left(f_{\rm met}\right) - G_{\rm met}\left(f_{\rm met}\right)}{G_{\rm e,M\text{-}G\text{-}2}\left(f_{\rm met}\right) + G_{\rm met}\left(f_{\rm met}\right)} = \left(100\% - f_{\rm met}\right)\frac{G_{\rm ins}\left(f_{\rm met}\right) - G_{\rm met}\left(f_{\rm met}\right)}{G_{\rm ins}\left(f_{\rm met}\right) + G_{\rm met}\left(f_{\rm met}\right)}, \tag{10}$$

Table 2: Experimental data in the warming and cooling processes [19]. Note that $G_{\rm met}$ and $G_{\rm ins}$ cannot be obtained directly through experiments. We get the data by extrapolating G near the warming and cooling driven phase transition processes.

Warming process					Cooling process				
T (K)	$f_{\rm met}$ (%)	G (s)	$G_{\rm met}$ (s)	$G_{\rm ins}$ (s)	T (K)	$f_{\rm met}$ (%)	G (s)	$G_{\rm met}$ (s)	$G_{\rm ins}$ (s)
161	0.928	0.002	0.138973	0.002021	158	2.831	0.008	0.138788	0.002966
164	16.009	0.008	0.141131	0.003616	161	27.100	0.016	0.140805	0.004387
167	53.921	0.027	0.143289	0.005211	164	51.787	0.027	0.142823	0.005808
170	62.506	0.050	0.145447	0.006806	167	61.253	0.053	0.144840	0.007230
173	76.798	0.075	0.147605	0.008401	170	66.125	0.083	0.146857	0.008651
176	89.559	0.100	0.149763	0.009996	173	81.578	0.108	0.148874	0.010072
179	95.824	0.124	0.151921	0.011591	176	95.545	0.132	0.150891	0.011494
182	99.814	0.145	0.154079	0.013186	179	99.118	0.148	0.152909	0.012915

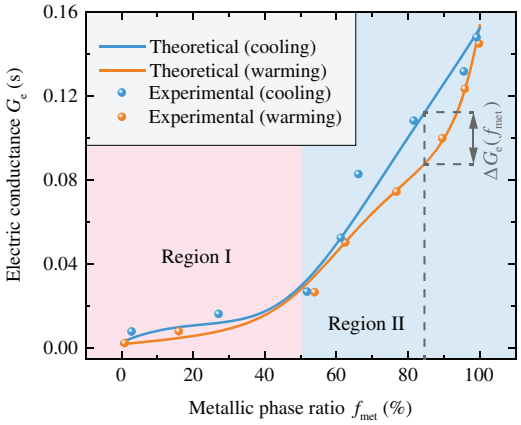

Fig. 2: Relationships between $G_{\rm e}$ and $f_{\rm met}$ in the warming and cooling processes. The experimental data is extracted from ref. [19]. Note that the grey lines are added to introduce the calculation method of the electric conductance difference $\Delta G_{\rm e}(f_{\rm met})$ during warming and cooling processes. The detailed calculation approach reads $\Delta G_{\rm e}(f_{\rm met}) = G_{\rm e}^{\rm c}(f_{\rm met}) - G_{\rm e}^{\rm w}(f_{\rm met})$, where $G_{\rm e}^{\rm c}(f_{\rm met})$ and $G_{\rm e}^{\rm w}(f_{\rm met})$ denote $G_{\rm e}(f_{\rm met})$ in the cooling and warming processes, respectively. For more details, see fig. 5. In addition, the slight difference of $G_{\rm e}$ during warming and cooling processes observed in $f_{\rm met} = 50\%$ is caused by the different $G_{\rm met}(f_{\rm met})$ and $G_{\rm ins}(f_{\rm met})$ during warming and cooling processes (table 2).

where $G_{\rm e,M\text{-}G\text{-}2}$ is the effective electric conductance calculated by the M-G-2 formula. Replacing the M-G-1 formula in the warming process with the M-G-2 formula, the rest calculation methods of $G_{\rm e}(f_{\rm met})$ in the cooling process are the same as those in the warming process, as stated above.

Experimental fitting. – Now, let us verify the above theory. We extract the detailed relationships among $G_{\rm met}$, $G_{\rm ins}$, T, and $f_{\rm met}$ in the warming and cooling processes from the experimental data, as listed in table 2. We obtain $G_{\rm met}(f_{\rm met})$ and $G_{\rm ins}(f_{\rm met})$ by extrapolations. Using eqs. (4), (6), and (8)–(10), we finally plot $G_{\rm e}(f_{\rm met})$ in the warming/cooling process, as shown in fig. 2. Considering the three typical steps (eq. (7)), we divide the curves into two regions: $f_{\rm met} \in$ [0%–50%] (region I) and $f_{\rm met} \in$ [50%–100%] (region II). When $f_{\rm met}$ rises from 0% to 50%, the electric conductance difference $\Delta G_{\rm e}(f_{\rm met})$ in the warming and cooling processes increases and then decreases. A similar and more significant phenomenon occurs when $f_{\rm met}$ rises from 50% to 100%. It reproduces the hysteresis of $G_{\rm e}$ against $f_{\rm met}$ in ref. [19].

Discussion and conclusion. – We first reveal the hysteresis of $G_{\rm e}$ against $f_{\rm met}$. In the warming process, the host (insulating phase) in the M-G-1 formula (eq. (4)) isolates the inclusion (metallic phase). However, in the cooling process, the host (metallic phase) in the M-G-2 formula (eq. (10)) is not entirely blocked by the inclusion (insulating phase). Compared to the warming process, the cooling process is more straightforward for the current to pass through. Thus, when $f_{\rm met} \in (0\%, 50\%) \cup (50\%, 100\%)$, $G_{\rm e}$ in the cooling process is larger than in the warming process. This analysis is compatible with the domain evolution explanation in ref. [19]. When $f_{\rm met} = f_{\rm ins} = 50\%$, the metallic and insulating phases are exchangeable. The contributions of the metallic phase and the insulating phase to $G_{\rm e}$ are equal, consistent with percolating theory [19]. The Bruggeman formula (eq. (6)) with symmetrical characteristics is more accurate in describing this situation. Our theoretical predictions agree with the experimental results by smoothly combining the M-G-1 (M-G-2) formula and the Bruggeman formula (fig. 2). It indicates that the hysteresis of $G_{\rm e}(f_{\rm met})$ is due to the hybrid impacts of phase symmetry and asymmetry.

We then discuss a potential application of our theory. It is known that $G(T)$ can be measured experimentally. $G_{\rm met}(T)$ and $G_{\rm ins}(T)$ are inherent properties of the material. Meanwhile, our theory can obtain $G_{\rm e}(f_{\rm met})$ (eq. (8)). Setting $G(T) = G_{\rm e}(f_{\rm met})$, we get $f_{\rm met}(T)$, as shown in fig. 3. It is consistent with the experimental results obtained by scanning microwave impedance microscopy [19]. It means we can predict the nucleation and

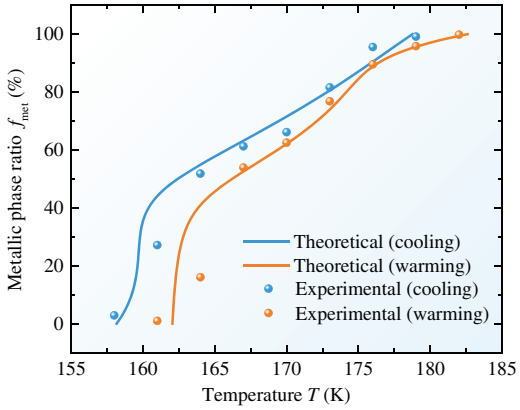

Fig. 3: Relationships between $f_{\rm met}$ and T in the warming and cooling processes. The experimental data is extracted from ref. [19].

growth behavior of the minority phase in the majority phase during phase transition to some extent. Compared to the warming process, the $f_{\rm met}$ in the cooling process is significantly larger at the same T. The result shows that the nucleation and growth behaviors during the warming and cooling processes are asymmetrical.

We further explore the thermal hysteresis mechanism. Combining $G_{\rm e}\left(f_{\rm met}\right)$ and $f_{\rm met}\left(T\right)$, we obtain $G_{\rm e}(T)$, as shown in fig. 4(a). There exists around 3.3–4.1 K thermal hysteresis during warming and cooling processes. Since the evolution of the $G_{\rm e}$ against T contains the influence of $G_{\rm e}\left(f_{\rm met}\right)$ and $f_{\rm met}\left(T\right)$, we attribute the thermal hysteresis of $G_{\rm e}(T)$ (or $R(T)$ in ref. [19]) to two factors. The first is the hybrid impacts of phase symmetry and asymmetry (fig. 2). It reflects the influence of the spatial distribution of the metallic and insulating phases on $G_{\rm e}$ during the phase transition. We term it a space factor. The second is the asymmetrical behavior of minority phase, which nucleates and grows in the majority phase during warming and cooling processes (fig. 3). It reveals the asymmetrical dynamic behavior during warming and cooling processes. We regard it as a dynamic factor. To go further, we provide quantitative analysis. Figure 4(b) indicates that the electric conductance differences $\Delta G_{\rm e}(T)$ is a crucial parameter of the thermal hysteresis magnitude. The more the $\Delta G_{\rm e}(T)$, the more significant the thermal hysteresis magnitude. We calculate $\Delta G_{\rm e}$ of $G_{\rm e}\left(f_{\rm met}\right)$ and $G_{\rm e}(T)$ during warming and cooling processes, as shown in fig. 5. It shows the contributions of the space factor and the dynamic factor to $\Delta G_{\rm e}\left(f_{\rm met}\right)$ and $\Delta G_{\rm e}(T)$. Note that $\Delta G_{\rm e}\left(f_{\rm met}\right)$ is only caused by the space factor, as mentioned above. In comparison, $G_{\rm e}(T)$ contains $G_{\rm e}\left(f_{\rm met}\right)$ and $f_{\rm met}(T)$, so $\Delta G_{\rm e}(T)$ is influenced by both space and dynamic factors. Therefore, $\Delta G_{\rm e}$ *vs.* T is more significant than $\Delta G_{\rm e}$ *vs.* $f_{\rm met}$. In short, the thermal hysteresis is owing to the asymmetrical elements of space and dynamic factors during phase transition.

The above discussion indicates that adjusting the asymmetrical elements in the above space and dynamic factors

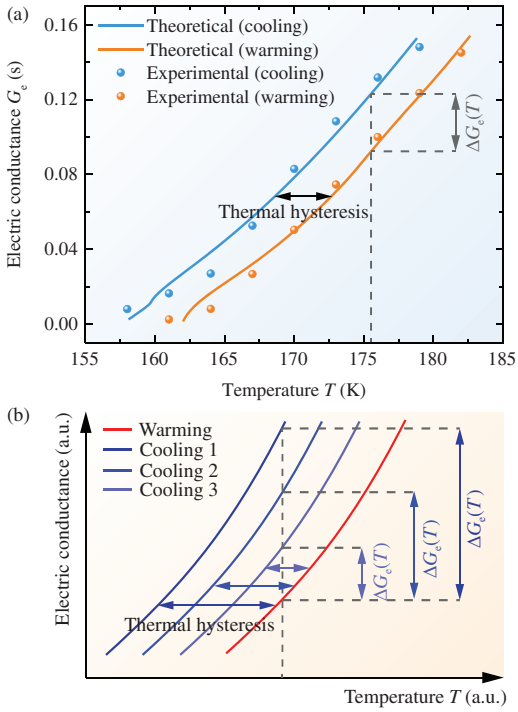

Fig. 4: (a) Relationships between $G_{\rm e}$ and T in the warming and cooling processes. The experimental data is extracted from the ref. [19]. Note that the grey lines are added to introduce the calculation method of the electric conductance difference $\Delta G_{\rm e}(T)$. The detailed calculation approach reads $\Delta G_{\rm e}\left(T\right) = G_{\rm e}^{\rm c}\left(T\right) - G_{\rm e}^{\rm w}\left(T\right)$, where $G_{\rm e}^{\rm c}\left(T\right)$ and $G_{\rm e}^{\rm w}\left(T\right)$ denote $G_{\rm e}\left(T\right)$ in the cooling and warming processes, respectively. For more details, see fig. 5. (b) Schematic diagram of the relationships between $\Delta G_{\rm e}(T)$ and thermal hysteresis magnitude. We keep the warming process unchanged and show the effect of different cooling processes on $\Delta G_{\rm e}(T)$ and the thermal hysteresis magnitude. The increasing thermal hysteresis magnitude leads to the rising $\Delta G_{\rm e}(T)$.

during phase transitions is key to regulating thermal hysteresis magnitude in practical applications. Doping methods can achieve this goal [39–41]. Adding some extra substances might adjust the nucleation and growth processes of the minority phase in the majority phase. For instance, ref. [41] used W-Ti doping to optimize the electrical performance of the V_2O_3 sample. The obtained co-doped V_2O_3 film has no hysteresis loops during phase transition. Interestingly, this mechanism and experimental approach exist not only in metal-insulator transitions. In the solid-liquid transitions, researchers controlled the hysteresis magnitude through various additives for realizing stable thermal energy release or seasonal thermal energy storage [15,16,42–45]. For example, ref. [43] reported a novel composite phase change material with stable heat release performance. Although a large thermal hysteresis exists during the solid-liquid transition, the suitable solidification temperature allows the material to be used for thermal energy utilization in daily life. For more phase transitions in different systems [6,7,46–48],

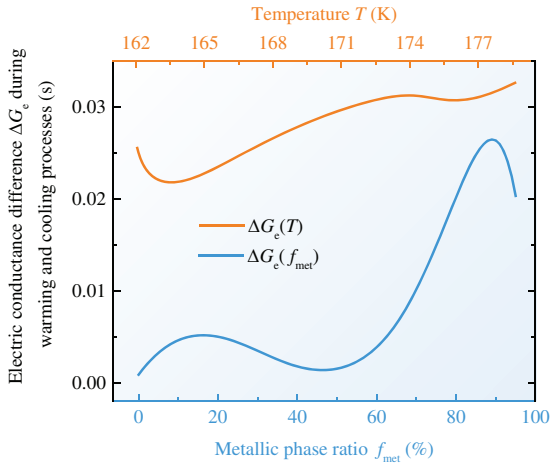

Fig. 5: Electric conductance differences ΔG_e during the warming and cooling processes. The blue line is the relationship between ΔG_e and f_{met}, corresponding to fig. 2. The orange line is the relationship between ΔG_e and T, which corresponds to fig. 4(a). Note that the calculation methods of $\Delta G_e\,(f_{met})$ and $\Delta G_e\,(T)$ are shown in fig. 2 and fig. 4(a), respectively. For ease of presentation, we take the ranges of f_{met} and T as [0%, 95%] and [162.1 K, 178.6 K], respectively.

the electric conductance in our theory can be replaced by corresponding physical properties such as thermal conductivity [20–22], dielectric constant [25], and magnetic permeability [29]. Therefore, this work may have broad application prospects.

In summary, we established an effective medium theory to predict the relationship between the effective electric conductance G_e and metallic phase ratio f_{met} during phase transition in the V_2O_3 system. It reveals that the hysteresis of $G_e\,(f_{met})$ is due to the hybrid impacts of phase symmetry and asymmetry in spatial distribution (termed space factor). We then applied this theory to predict the evolution of f_{met} with temperature T. It shows that the nucleation and growth behaviors of the minority phase in the majority phase during the warming and cooling processes are asymmetrical (termed dynamic factor). Since $G_e(T)$ contains $G_e\,(f_{met})$ and $f_{met}(T)$, we attributed the thermal hysteresis of $G_e(T)$ to the space factor and the dynamic factor. To go further, we analyzed the influence of these two factors on the electric conductance difference ΔG_e during warming and cooling processes. It indicates that the thermal hysteresis magnitude can be controlled by regulating the asymmetrical elements in the space and dynamic factors. Since hysteresis exists in various phase transition processes [10–16], this work might be helpful in many situations for analyzing different phase transition behaviors.

* * *

We are grateful to Mr. H. Y. Zhang for beneficial discussion. JPH, XCZ, and FBY acknowledge financial support from the National Natural Science Foundation of China under Grants No. 11725521 and No. 12035004, and from the Science and Technology Commission of Shanghai Municipality under Grant No. 20JC1414700. XDZ acknowledges support from National Natural Science Foundation of China under Grants No. 12074080 and No. 11804052, and from Shanghai Science and Technology Committee Rising-Star Program (19QA1401000).

REFERENCES

[1] Shen N., Chen S., Shi R., Niu S., Amini A. and Cheng C., *ACS Appl. Electron. Mater.*, **3** (2021) 3648.
[2] Shen N., Chen S., Huang R., Huang J., Li J., Shi R., Niu S., Amini A. and Cheng C., *Mater. Today Energy*, **21** (2021) 100827.
[3] Ge G., Shi C., Chen C., Shi Y., Yan F., Bai H., Yang J., Lin J., Shen B. and Zhai J., *Adv. Mater.*, **34** (2022) 2201333.
[4] Qiu Q., Yang S., Gerkman M. A., Fu H., Aprahamian I. and Han. G. G. D., *J. Am. Chem. Soc.*, **144** (2022) 12627.
[5] Lin N., Li C., Zhang D., Li Y. and Chen J., *Energy*, **245** (2022) 123294.
[6] Zhang X., Tong P., Lin J., Tao K., Wang X., Xie L., Song W. and Sun Y., *Phys. Rev. Appl.*, **16** (2021) 014031.
[7] Jacobs M., Zhou X., Olivera E., Sheil R., Huang S., Marszewski M., Chang J., Tolbert S., Osher S., Pilon L. and Marian J., *J. Appl. Phys.*, **129** (2021) 075103.
[8] Aryana K., Gaskins J. T., Nag J., Stewart D. A., Bai Z., Mukhopadhyay S., Read J. C., Olson D. H., Hoglund E. R., Howe J. M., Giri A., Grobis M. K. and Hopkins P. E., *Nat. Commun.*, **12** (2021) 774.
[9] Gallo M. L. and Sebastian A., *J. Phys. D: Appl. Phys.*, **53** (2020) 213002.
[10] Hu T., Fu Z., Li Z., Liu M., Zhang L., Yu Z., Chen X., Zheng Y., Li T., Wang Y., Wang G., Dong X. and Xu F., *ACS Appl. Mater. Interfaces*, **13** (2021) 60241.
[11] Li Z., Wu H.-H., Li J., Wang S., Qin S., He J., Liu C., Su Y., Qiao L., Lookman T. and Bai Y., *Acta Mater.*, **228** (2022) 117784.
[12] Ma Y., Chen R., Li Y., Lu C. and Zhang C., *Phys. Rev. B*, **105** (2022) 155110.
[13] Mohammadzadeh A., Baraghani S., Yin S., Kargar F., Bird J. P. and Balandin A. A., *Appl. Phys. Lett.*, **118** (2021) 093102.
[14] Pang E. L., Olson G. B. and Schuh C. A., *Acta Mater.*, **213** (2021) 116972.
[15] Liu L., Zhang X. and Lin X., *Renew. Energy*, **187** (2022) 572.
[16] Barz T. and Sommer A., *Int. J. Heat Mass Transfer*, **127** (2018) 701.
[17] Ha J.-H., Kim H.-W., Jo Y.-S., Kim S.-W. and Hong J.-I., *Appl. Mater. Today*, **22** (2021) 100984.
[18] Mazzola F., Chaluvadi S. K., Polewczyk V., Mondal D., Fujii J., Rajak P., Islam M., Ciancio R., Barba L., Fabrizio M., Rossi G., Orgiani P. and Vobornik I., *Nano Lett.*, **22** (2022) 5990.

[19] Lin W., Zhang H., Kalcheim Y., Zhou X., Yang F., Shi Y., Feng Y., Wang Y., Huang J., Schuller I. K., Zhou X. and Shen J., *Sci. China: Phys. Mech. Astron.*, **65** (2022) 297411.
[20] Tian B., Wang J., Dai G., Ouyang X. and Huang J., *Int. J. Heat Mass Transfer*, **174** (2021) 121312.
[21] Wang C. Q., Xu L. J., Jiang T., Zhang L. and Huang J. P., *EPL*, **133** (2021) 20009.
[22] Huang T., Yang F., Wang T., Wang J., Li Y., Huang J., Chen M. and Wu L., *Appl. Mater. Today*, **26** (2022) 101299.
[23] Wen Z., Xu H., Zhao W., Zhou Z., Li X., Li S., Zhou J., Sun Y., Dai N. and Hao J., *J. Opt.*, **23** (2021) 065103.
[24] Gao Y., Huang J. P., Liu Y. M., Gao L., Yu K. W. and Zhang X., *Phys. Rev. Lett.*, **104** (2010) 034501.
[25] Huang J. P. and Yu. K. W., *Phys. Rep.-Rev. Sect. Phys. Lett.*, **431** (2006) 87.
[26] Aouaichia M., McCullen N., Bowen C. R., Almond D. P., Budd C. and Bouamrane R., *Eur. Phys. J. B*, **90** (2017) 39.
[27] Nigro B., Grimaldi C. and Ryser P., *Phys. Rev. E*, **85** (2012) 011137.
[28] Papadakis G. T., Yeh P. and Atwater H. A., *Phys. Rev. B*, **91** (2015) 155406.
[29] Jin J., Liu S., Lin Z. and Chui S. T., *Phys. Rev. B*, **80** (2009) 115101.
[30] Grimstad G., Ghoreishian S. A. and Nordal S., *Front. Phys.*, **7** (2019) 41.
[31] Salimi H., Bruining J. and Joekar-Niasar V., *J. Pet. Sci. Eng.*, **184** (2020) 106594.
[32] Maxwell Garnett J. C., *Philos. Trans. R. Soc. London Ser. A*, **203** (1904) 385.
[33] Maxwell Garnett J. C., *Philos. Trans. R. Soc. London Ser. A*, **205** (1906) 237.
[34] Zhou X.-F. and Gao L., *Chin. Phys.*, **16** (2007) 2028.
[35] Miao X. P., Gao L. and Xu P., *J. Appl. Phys.*, **103** (2008) 023512.
[36] Sun J., Huang Y. and Gao L., *Phys. Rev. A*, **89** (2014) 012508.
[37] Bruggeman D. A. G., *Ann. Phys. (Berlin)*, **24** (1935) 636.
[38] Huang J. P., *Theoretical Thermotics: Transformation Thermotics and Extended Theories for Thermal Metamaterials* (Springer) 2020.
[39] Korde V., Patil N. and Shamkuwar S., *Ceram. Int.*, **48** (2022) 9172.
[40] Ge J., Hong J., Liu T. and Wang Y., *J. Mater. Chem. A*, **10** (2022) 11458.
[41] Sun G., Cao X., Long S., Li R. and Jin P., *Appl. Phys. Lett.*, **111** (2017) 053901.
[42] Que L., Zhang X., Ji J., Gao L., Xie W., Liu L. and Ding X., *Energy Build.*, **253** (2021) 111402.
[43] Zhou X., Zhang X. and Zheng Q., *Sol. Energy Mater. Sol. Cells*, **217** (2020) 110725.
[44] Zhou X., Zhang X. and Zheng Q., *Energy Fuels*, **34** (2020) 7607.
[45] Ma Z., Bao H. and Roskilly A. P., *Sol. Energy Mater. Sol. Cells*, **172** (2017) 99.
[46] Dehno R. T. and Khoshnoud D. S., *J. Magn. & Magn. Mater.*, **541** (2022) 168515.
[47] Mishra S., Sahoo A., Mondal S., Mandal P., Ghosh C. K. and Bhattacharya D., *J. Appl. Phys.*, **131** (2022) 204101.
[48] Galdun L., Vidyasagar R., Hennel M., Varga M., Ryba T., Nulandaya L., Milkovic O., Reiffers M., Kravcak J., Vargova Z. and Varga R., *J. Phys. D: Appl. Phys.*, **55** (2022) 045303.